

# Kinetics and morphology of cluster growth in a model of short-range attractive colloids

Siddique J. Khan, C. M. Sorensen, and A. Chakrabarti<sup>a)</sup>

*Department of Physics, Kansas State University, Manhattan, Kansas 66503, USA*

(Received 31 August 2009; accepted 19 October 2009; published online 19 November 2009)

We present results from detailed three-dimensional Brownian dynamics simulations of the self-assembly process in quenched short-range attractive colloids. Clusters obtained in the simulations range from dense faceted crystals to fractal aggregates which show ramified morphology on large length scales but close-packed crystalline morphology on short length scales. For low volume fractions of the colloids, the morphology and crystal structure of a nucleating cluster are studied at various times after the quench. As the volume fraction of the colloids is increased, growth of clusters is controlled by cluster diffusion and cluster-cluster interactions. For shallower quenches and low volume fractions, clusters are compact and the growth-law exponent agrees well with Binder–Stauffer predictions and with recent experimental results. As the volume fraction is increased, clusters do not completely coalesce when they meet each other and the kinetics crosses over to diffusion-limited cluster-cluster aggregation (DLCA) limit. For deeper quenches, clusters are fractals even at low volume fractions and the growth kinetics asymptotically reaches the irreversible DLCA case. © 2009 American Institute of Physics. [doi:[10.1063/1.3262311](https://doi.org/10.1063/1.3262311)]

## I. INTRODUCTION

Self-assembly in colloidal<sup>1</sup> and nanoparticle<sup>2</sup> systems is governed by a rich series of phase transitions between colloidal gas, liquid, and solid phases. The liquid phase can be amorphous or liquid crystalline and the solid phases can be crystalline, amorphous (often fractal), and gel. These possibilities are controlled by the details of the potential between the disperse components, on one hand, and the kinetics of the phase transition, on the other. A fluid to crystal transition occurs if the potential is solely hard sphere. Addition of an attractive potential brings on three phase equilibria. A key parameter that affects large changes of the phase diagram is the *relative range* of the attractive interaction between the colloidal particles. For short-range attractive potentials, the system develops a gas-crystalline coexistence with a metastable liquid-liquid coexistence region. The presence of such a metastable liquid-liquid coexistence region affects the kinetics of nucleation and growth of clusters in colloidal and protein solutions.<sup>3</sup> In addition, kinetics of cluster growth in colloidal systems with short-range attractions<sup>4</sup> has striking similarity with other phase changes such as spinodal decomposition in binary mixtures of molecular systems<sup>5</sup> and the formation of precipitated crystalline solids from solutions.<sup>6</sup> Thus, colloidal systems are of fundamental interest for a detailed understanding of how a dispersed phase, such as particles in a colloid or molecules in a solution, comes together when destabilized and forms a condensed phase such as aggregates, gels, or crystalline solids. Parts of this grand problem have seen considerable previous research such as irre-

versible aggregation and the formation of fractal aggregates,<sup>7</sup> gelation,<sup>8</sup> spinodal decomposition,<sup>5</sup> nucleation,<sup>9</sup> and early studies of growth during precipitation.<sup>6</sup> However, a general theory that encompasses all these related phenomena is lacking.

Phase behavior of short-range attractive colloids has been studied extensively both theoretically and experimentally. The equilibrium behavior of these systems being reasonably well understood, recent attention has been directed to the understanding of kinetics of phase transitions and colloidal gelation<sup>8</sup> and its relation to glass transition and the more general jamming transition.<sup>9,10</sup> Hobbie<sup>11</sup> studied the growth kinetics of the crystallization process in depletion driven colloids and compared experimental results with mean-field theories of aggregation-fragmentation.<sup>12</sup> Direct observation of crystallization and aggregation, on one hand, and sublimation of these crystals, on the other, has been carried out by de Hoog *et al.*<sup>13</sup> and more recently by Savage *et al.*<sup>14</sup> by varying the depth of the depletion potential. Arrested spinodal decomposition and the formation of solidlike network in colloids and protein solutions were studied by several groups.<sup>15–17</sup> A recent work by Lu *et al.*<sup>15</sup> suggested that gelation in short-range attractive colloids starts from density fluctuations (en route to spinodal decomposition) that get dynamically arrested. Computer simulations have also been carried out to study transient gel formation and crystallization in these systems. Evidence of metastability, homogeneous nucleation, kinetically arrested gel state, and density instability was reported in various simulations.<sup>15,18–22</sup> In addition, simulations strongly suggest that kinetic behaviors in short-range attractive colloids<sup>15</sup> do not depend on microscopic details but generally apply to any particle system with short-range attractions.<sup>23</sup>

<sup>a)</sup>Author to whom correspondence should be addressed. Electronic mail: amitc@phys.ksu.edu.

In this paper, we present results from extensive Brownian dynamics (BD) simulations for a system of colloidal particles interacting via a short-range attractive potential. To demonstrate our general results with a specific example, we consider the Asakura–Oosawa–Vrij (AOV) model of depletion interaction<sup>24,25</sup> which approximately accounts for the interaction between a pair of colloidal particles by an effective two-body interaction. We focus on lower monomer concentrations and study the kinetics and morphology of cluster growth in large-scale three-dimensional simulations. In the context of recent experiments by Lu *et al.*<sup>15</sup> mentioned above, how the cluster growth kinetics changes as one increases the volume fraction and the depth of the potential well will be of particular interest. This is studied in our large-scale simulations.

Clusters obtained in the simulations range from dense faceted crystals to fractal aggregates which show ramified morphology on large scales but close-packed crystalline morphology on short length scales. For low volume fractions, the morphology and crystal structure of a nucleating cluster are studied at various times after the quench. As the volume fraction of the colloids is increased, growth of clusters is controlled by cluster diffusion and cluster-cluster interactions. For shallower quenches and low volume fractions, clusters are compact and the growth-law exponent agrees well with theoretical predictions<sup>26,27</sup> and with recent experimental results.<sup>15</sup> As the volume fraction is increased, clusters do not coalesce when they meet each other and the kinetics crosses over to the diffusion-limited cluster-cluster aggregation<sup>28</sup> (DLCA) limit. For deeper quenches, clusters are fractals even at low volume fractions and the growth kinetics asymptotically reaches the irreversible case, namely, the DLCA. Fractal clusters observed in our simulations have a hybrid structure<sup>29,30</sup> with a closed-packed crystalline ordering at short length scales and a ramified morphology at larger length scales.

The rest of the paper is organized as follows. In Sec. II we describe the model and numerical method employed in our work. In Sec. III we present simulation results. First, we study the crystalline morphology of the nucleating and growing cluster. Next, we study the growth kinetics of clusters and compare them with cluster growth in spinodal decomposition of binary systems and with DLCA models. We also study the morphology of the clusters at various length scales. Finally, we conclude in Sec. IV with a brief summary and discussion of the results.

## II. MODEL AND SIMULATION METHOD

In our BD simulations,<sup>31</sup> we consider three-dimensional systems of sizes  $L=128\sigma$  in units of monomer diameter  $\sigma$ . All other length scales are measured in units of  $\sigma$  as well. We consider a wide range of monomer volume fractions from  $f=0.0001$  to  $0.02$ , with the number of monomers ranging up to  $N_m=84\,000$ .

The equations of motion for the BD simulation read as

$$\ddot{\vec{r}}_i = -\vec{\nabla}U_i - \Gamma\dot{\vec{r}}_i + \vec{W}_i(t), \quad (1)$$

where  $\Gamma$  is the friction coefficient and  $W_i$ , the random force acting on each colloidal particle  $i$ , is a Gaussian white noise satisfying a fluctuation-dissipation relation. Hydrodynamic interactions, including lubrication forces, are ignored in the simulation as they might not be of predominant importance for a study of quiescent secondary minimum colloids.<sup>32</sup> The potential  $U$  acting upon each colloidal particle has a twofold contribution: the two-body depletion potential of AOV ( $U_{AO}$ ) plus a repulsive hard-core-like interaction ( $U_{hc}$ ) given by the following expressions:

$$U(r_{ij}) = U_{AO}(r_{ij}) + U_{hc}(r_{ij}), \quad (2)$$

where

$$\frac{U_{AO}(r_{ij})}{kT} = \begin{cases} \phi_p \left( \frac{1+\xi}{\xi} \right)^3 \left[ \frac{3}{2} \frac{r_{ij}}{1+\xi} - \frac{1}{2} \left( \frac{r_{ij}}{1+\xi} \right)^3 - 1 \right] & \text{for } r_{ij} < (1+\xi) \\ 0 & \text{for } r_{ij} > (1+\xi) \end{cases}, \quad (3)$$

and

$$\frac{U_{hc}(r_{ij})}{kT} = r_{ij}^{-\alpha}. \quad (4)$$

In Eq. (3),  $\xi$  is the size ratio between a polymer coil and a colloidal particle which controls the range of the depletion interaction in the AOV model and  $\phi_p$  is the polymer volume fraction which controls the strength of the interaction. Most of our simulations are for  $\xi=0.03$  and  $0.1$ , while some simulations have also been carried out for  $\xi=0.06$ . In the hard-core-like repulsive interaction given by Eq. (4), we have set  $\alpha=36$ . Exponents  $\alpha < 36$  are reported to lead to anomalies

when a hard-core mimic is required in the potential.<sup>18,33</sup> The total pair potential  $U=U_{AO}+U_{hc}$  passes through a minimum value ( $U_{min}$ ) that depends on  $\xi$  and  $\phi_p$ . In what follows, we will often characterize the strength of the potential in terms of the absolute value of the minimum potential depth,  $U_m=|U_{min}|$ . We choose  $\Gamma=0.5$  and time step  $\Delta t=0.005$  in reduced time units of  $\sigma(m/kT)^{1/2}$  with  $m=1$ . For this choice of  $\Gamma$ , particle motion is purely diffusive for  $t \gg 1/\Gamma$ , i.e.,  $t \gg 2$  in our units. Periodic boundary conditions are enforced to minimize wall effects. All simulations start from a random initial monomer conformation and the results for the kinetics are averaged over several (five to ten) runs.

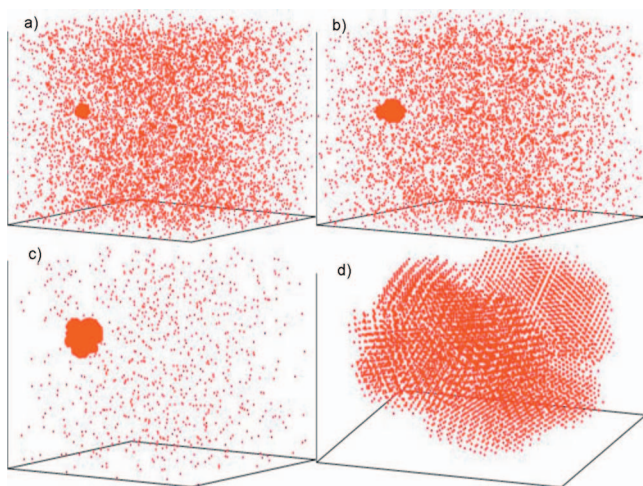


FIG. 1. Nucleating cluster for  $U_m=4kT$ ,  $\xi=0.03$ , and  $f=0.002$  at different times: (a)  $t=15\,000$ , (b)  $t=20\,000$ , (c)  $t=40\,000$ , and (d) zoomed-in cluster at  $t=20\,000$ .

### III. RESULTS

#### A. Morphology of a nucleating crystal

For low volume fractions and a quench to  $U_m=4kT$ , nucleation of the solid phase from a dispersed phase starts to develop as one would expect from the phase diagram of the model system.<sup>34,35</sup> To study the morphology of the nucleating cluster, we fine tune the monomer concentration  $f$  such that only one round-shaped cluster grows in our simulation box. Snapshots of such a growing cluster (for  $\xi=0.03$  and  $f=0.002$ ) amidst the colloidal gas phase are shown in Fig. 1 at various times along with a zoomed-in version of the cluster at the latest time.

To characterize such a growing cluster at different times during the growth process, we compute the radius of gyration  $R_g$  and the perimeter radius  $R_p$  for the growing cluster. For a compact spherical cluster,  $R_p$  is related to  $R_g$  in the following way:

$$R_p = \sqrt{\frac{5}{3}} R_g. \quad (5)$$

We then define the *core* of the cluster as comprised of all particles residing at a distance  $\leq R_g$  from the center of mass and the *cluster surface* as a collection of all particles residing at a distance  $\geq R_p$  from the center of mass. Next we calculate the distance of the  $i$ th nearest neighbor (NN) of each particle and average over the core and surface particles separately. This is shown in Fig. 2 for clusters at early and late times. Since the potential minimum for  $\xi=0.03$  [see Eqs. (2)–(4)] is at  $r_{\min}=0.95$ , the first NN is located at this distance. At the latest time, the cluster core shows 12 NN within a small spread of distance indicating a closed packed crystal structure (fcc or hcp). A subsequent discontinuity in distance indicates the beginning of the next NN sequence and six such next NNs follow. Another weak discontinuity comes next and then the sequence of 12 third NNs follows. In contrast, at earlier times, the growing cluster has only five or six pure NNs at separation  $r_{\min}=0.95$  and then a sequence of neighbors whose distance increases continuously. As also shown in Fig. 2, this *liquidlike* morphology of the cluster at early

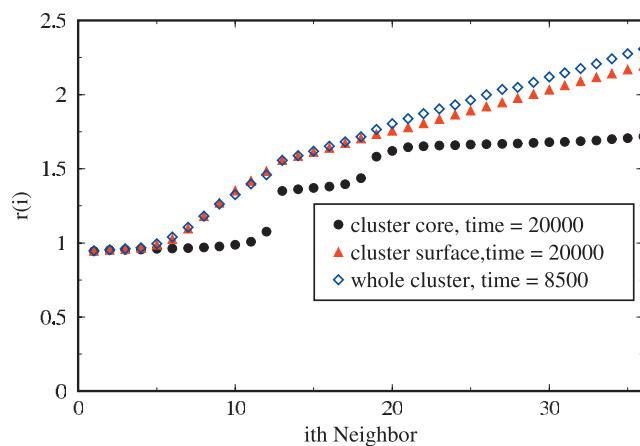


FIG. 2. Plot of average distance  $r(i)$  of the  $i$ th neighbor for particles in the nucleating cluster for  $U_m=4kT$ ,  $f=0.002$ , and  $\xi=0.03$ .

times is strikingly similar to the surface structure of the cluster at late times.

The crystalline nature of the droplet at late times is evident in the data for the radial distribution function  $g(r)$  shown in Fig. 3. We define the *NN distance*  $\delta$  as the location of the first minimum of  $g(r)$ .<sup>36</sup> This distance  $\delta$  actually coincides with the location of the first discontinuity in the neighbor distances plotted in Fig. 2. The number of near neighbors of a particle  $i$  within  $\delta$  is denoted as  $N_b(i)$  and is used in our calculations of various bond orientational orders described in the following.

Next we compute local bond order parameters for particles in the growing cluster. For this purpose, we follow an algorithm based on spherical harmonics originally proposed by Steinhardt *et al.*<sup>37</sup> and successfully employed by Auer and Frenkel.<sup>38</sup> More recently, such analysis has also been carried out for colloidal gels.<sup>39,40</sup> We first associate spherical harmonics with all the neighbors of each particle in the cluster and compute

$$q_{lm}(i) \equiv \frac{1}{N_b(i)} \sum_{j=1}^{N_b(i)} Y_{lm}(\hat{r}_{ij}). \quad (6)$$

Here  $\hat{r}_{ij}$  is the unit vector connecting particles  $i$  and  $j$  which uniquely determines the polar and azimuthal angles  $\theta_{ij}$  and

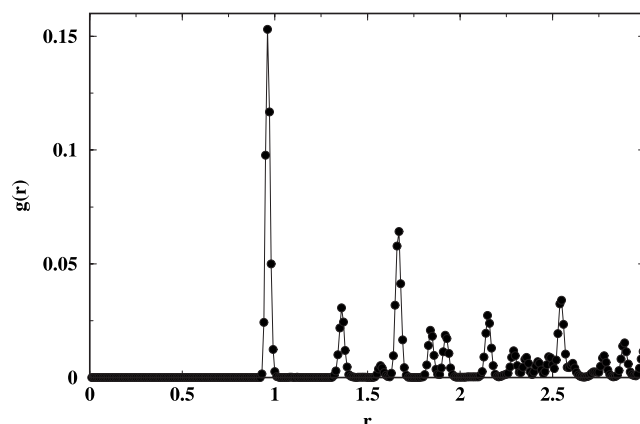


FIG. 3. Radial distribution function  $g(r)$  as a function of separation  $r$  between the particles of the nucleating cluster for  $U_m=4kT$ ,  $\xi=0.03$ , and  $f=0.002$  at  $t=20\,000$ .

TABLE I. Global bond order parameters for pure crystals.

	$Q_4$	$Q_6$
fcc	0.191	0.575
hcp	0.097	0.485
bcc	0.036	0.511
sc	0.764	0.354
Liquid	0	0

$\phi_{ij}$  which, in turn, can be used to compute the spherical harmonics  $Y_{lm}(\theta_{ij}, \phi_{ij}) \equiv Y_{lm}(\hat{r}_{ij})$ . The local order parameter  $q_l(i)$  is then defined as

$$q_l(i) \equiv \left[ \frac{4\pi}{2l+1} \sum_{m=-1}^l |\bar{q}_{lm}(i)|^2 \right]^{1/2}. \quad (7)$$

We compute this quantity for each particle  $i$  in the cluster (separately for core and surface sites) and then compute the probability (frequency) distribution functions for  $l=4$  and  $l=6$ . Rotationally invariant global order parameters can be defined from calculating averages of the local order parameters as

$$\bar{Q}_{lm} \equiv \frac{\sum_{i=1}^N N_b(i) \bar{q}_{lm}(i)}{\sum_{i=1}^N N_b(i)}, \quad (8a)$$

$$Q_l \equiv \left[ \frac{4\pi}{2l+1} \sum_{m=-1}^l |\bar{Q}_{lm}|^2 \right]^{1/2}. \quad (8b)$$

Values of  $Q_l$ , the global averaged orientation order parameter for pure crystal, occur for  $l=4$  and  $l=6$  as shown in the Table I. Note that  $Q_l$  is zero for liquids with  $l=4$  and  $l=6$ . We should note that to compute  $Q_l$ , we have used only NNs for fcc and hcp crystals [i.e.,  $N_b(i)=12$  for fcc and hcp] while for bcc, both NN and next NN are included in the calculation [i.e.,  $N_b(i)=14$  for bcc].

Our results for the frequency distribution  $P(q_6)$  for the cluster core are shown in Fig. 4. We observe that the crystal structure inside the core of the cluster is predominantly a mixture of fcc and hcp. Similar analysis of the bond orientational order of the surface sites at late times is compared

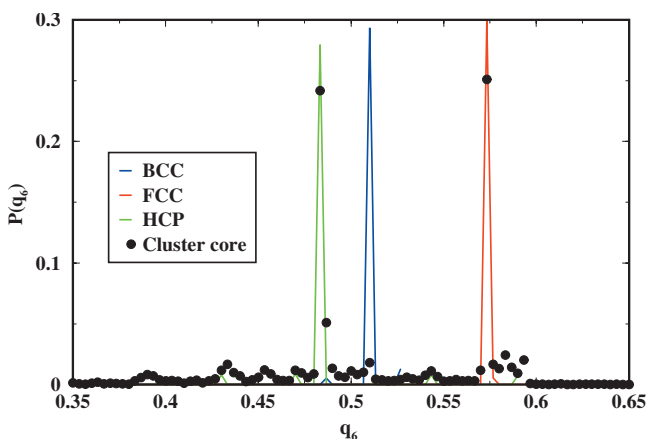


FIG. 4. Distribution of bond order parameter  $q_6$  for the nucleating cluster core in comparison with pure crystals of bcc, fcc, and hcp. Here  $t=40000$ ,  $\xi=0.03$ ,  $U_m=4kT$ , and  $f=0.002$ .

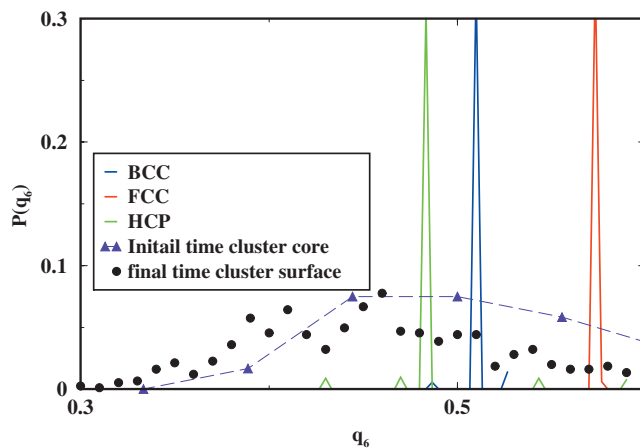


FIG. 5. Distribution of bond order parameter  $q_6$  for surface particles at a late time of  $t=40000$  of the nucleating cluster for  $U_m=4kT$ ,  $\xi=0.03$ , and  $f=0.002$  and its comparison with an early time cluster core at  $t=8500$ . Distribution for pure crystals of bcc, fcc, and hcp are also shown in the figure.

with the core of the growing cluster at early times in Fig. 5. From the broad distribution of the order parameters observed in Fig. 5, one can conclude that both the early time cluster core and the late time surface sites are liquidlike in structure. These results are in good agreement with experimental results obtained from real-space imaging of colloidal crystallization.<sup>41</sup> We do not see any evidence of a bcc structure either at early times or at the surface of the growing cluster at late times.<sup>42,43</sup> It seems that the hcp structure is more dominant at early stages while the fcc structure is dominant in the later stages. Our analysis for  $P(q_4)$  supports these conclusions.

## B. Morphology and growth kinetics for shallow quenches

In this section we continue with quenches to a depth of  $4kT$  but increase the volume fraction of the colloids. In Fig. 6 we show snapshots for the system at various times for  $f=0.005$  and  $\xi=0.1$ . Now several clusters nucleate and grow with time. The shape of the clusters is generally round for all values of  $\xi$ . When two clusters meet each other, it seems that

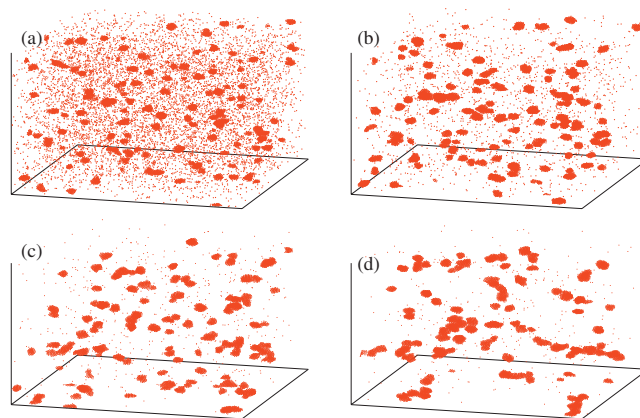


FIG. 6. Snapshots of the system for a  $U_m=4kT$  quench with  $f=0.005$  and  $\xi=0.1$  at different times: (a)  $t=1000$ , (b)  $t=2000$ , (c)  $t=5000$ , and (d)  $t=10000$ .

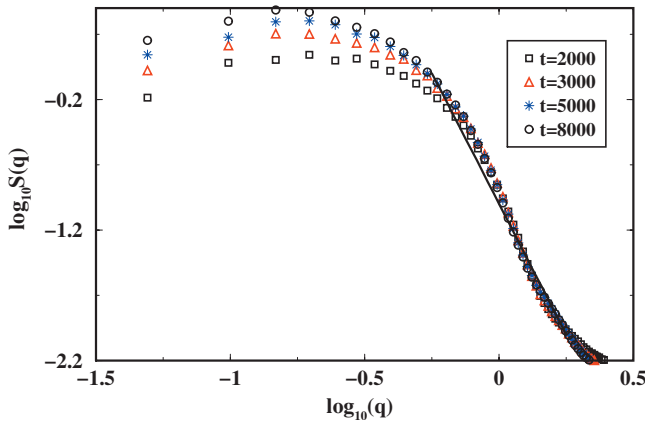


FIG. 7. Log-log plot of the structure factor  $S(q,t)$  as a function of  $q$  at different times for system with  $U_m=4kT$ ,  $f=0.005$ , and  $\xi=0.1$ . For large  $q$  values,  $S(q)$  is consistent with Porod's law although some deviations from  $q^{-4}$  form can be observed.

they have time to coalesce into one spherical droplet before another cluster is encountered. In Fig. 7 we show the log-log plot of the structure factor  $S(q,t)$  versus  $q$ . A fit to the data shows that  $S(q,t)$  is consistent with Porod's law<sup>44</sup> [ $S(q) \sim q^{-4}$ ] over a large range of  $k$  values, confirming our direct observations that the growing clusters are compact at both short and large length scales.

In Fig. 8 we show log-log plots of average radius of gyration  $R_g$  of the clusters as a function of time for  $\xi=0.03$  and  $\xi=0.1$ . Initially, we observe a sudden fast growth of  $R_g$  corresponding to heterogeneous nucleation of many clusters ( $100 \leq t \leq 1000$ ). Subsequently, these clusters grow with time with a power law

$$R_g \sim t^n, \quad (9)$$

with  $n \approx 0.17$ . As suggested by Binder and Stauffer<sup>26</sup> and Binder and Kalos<sup>27</sup> and later summarized by Gunton *et al.*<sup>5</sup> and Furukawa,<sup>45</sup> domain growth kinetics at this stage is mostly controlled by cluster diffusion until eventually two such clusters coalesce. The mechanics of cluster diffusion is dominated by *surface reorganization of the particles* in the cluster. Following Gunton *et al.*<sup>5</sup> we briefly summarize these arguments below.

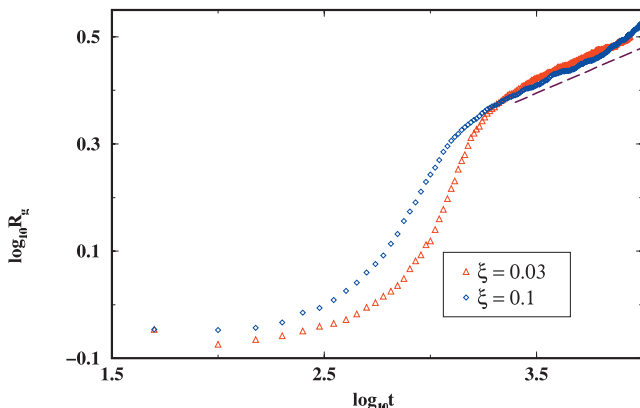


FIG. 8. Log-log plot of radius of gyration  $R_g$  as a function of time for  $f=0.005$ ,  $U_m=4kT$ , and two different  $\xi$  values (0.03 and 0.1). The dotted line with slope of 0.17 is a guide to the eyes.

The diffusion constant of a cluster containing  $N$  particles can be estimated as

$$D_N \approx \omega(\Delta x_G)^2, \quad (10)$$

where  $\Delta x_G$  is the change in the center of mass position by a given process of particle motion in the cluster and  $\omega$  is the rate at which such a process takes place. In a typical process of particle motion on the surface of a cluster, a particle changes its position by a few units of  $\sigma$ . As a result the center of mass of a cluster containing  $N$  particles changes by

$$\Delta x_G \approx N^{-1} \quad (11)$$

in units of  $\sigma$ . As the rate of such a particle motion at the surface is proportional to the number of surface sites, one estimates

$$\omega \approx R_g^2. \quad (12)$$

If the clusters are compact,  $R_g \sim N^{1/d}$ , where  $d$  is the spatial dimension. One thus obtains

$$D_N \approx N^{2/d-2}. \quad (13)$$

Once an estimate for cluster diffusion constant is obtained, one can now treat the cluster-cluster coalescence in terms of the mean-field Smoluchowski equation (SE)<sup>46,47</sup> which expresses the rate of change of cluster concentration,  $n_k(t)$ , containing  $k$  monomers per cluster as

$$\frac{dn_k}{dt} = \sum_{i=1}^{k-1} K(i, k-i) n_i n_{k-i} - n_k \sum_{i=1}^{\infty} K(i, k) n_i. \quad (14)$$

The kernel  $K(i,j)$  expresses the rate of aggregation or coalescence between clusters of size  $i$  with clusters of size  $j$ . If  $K$  is a homogeneous function of cluster size, i.e.,  $K(ai,aj) = a^\lambda K(i,j)$ , where  $\lambda$  is the degree of homogeneity, the solutions to the SE are self-preserving scaling solutions for  $n_k$ . If one further assumes that the cluster size distribution is approximately monodisperse, one can write the appropriate collision kernel as

$$K \sim N^\lambda. \quad (15)$$

The kinetic exponent  $z$ , which characterizes the power-law decay with time of the number of clusters  $N_c(t)$ , is related to the homogeneity  $\lambda$  by

$$z = \frac{1}{1-\lambda}. \quad (16)$$

In addition, since  $N_c N = \text{constant}$  (=the number of monomers), one easily finds that  $R_g(t) \sim t^n$ , where

$$n = z/d \quad (17)$$

for compact clusters.

The next step in this scaling description<sup>48,49</sup> is to pinpoint limiting cases of the functional form of the kernel and hence determine the homogeneity. The rate at which two clusters collide,  $K$ , is proportional to their relative *collision cross-sectional area*  $A$  and relative velocity,  $v$ , yielding  $K \sim Av$ , consistent with the units of  $[L^3/t]$ . One typically writes  $A$  as  $A \sim R_g^2$ , where  $R_g$  is the radius of gyration of a cluster with number of particles  $N$ . For the diffusive case of

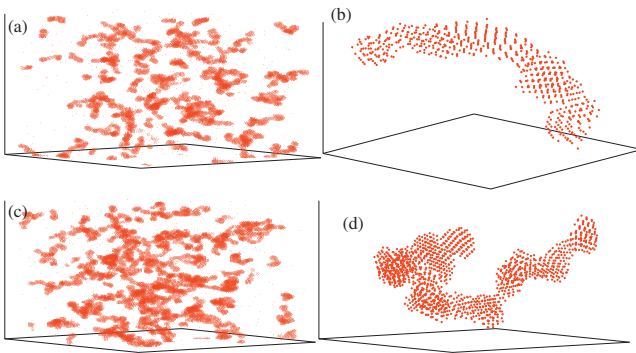


FIG. 9. Late time configuration for  $U_m=4kT$  and  $\xi=0.1$  for (a)  $f=0.01$  and (c)  $f=0.02$  at  $t=5000$ . A zoomed-in cluster for the corresponding cases are shown in (b)  $f=0.01$  and (d)  $f=0.02$ .

cluster motion,  $v$  becomes a *characteristic velocity relevant for diffusion*. This velocity must scale as

$$v \sim \frac{D_N}{R_c}, \quad (18)$$

where  $D_N$  is the diffusion constant of a cluster containing  $N$  particles and  $R_c$  is a characteristic diffusional length scale. In the dilute limit of the Stokes–Einstein diffusion,  $R_g$  is the only relevant length scale in the system and one can write  $v \sim D_N/R_g$ . In addition,  $A \sim R_g^2$ . Thus one finds  $K \sim D_N R_g$ , a result originally derived by Smoluchowski<sup>46</sup> in a more rigorous fashion.

For the Binder–Stauffer<sup>26</sup> cluster growth mechanism  $D_N \approx N^{2/d-2}$  and for compact clusters  $R_g \sim N^{1/d}$ . One thus finds

$$K \sim D_N R_g \sim N^{(2/d)-2+(1/d)} \sim N^{3/d-2}. \quad (19)$$

Hence the homogeneity

$$\lambda = \frac{3}{d} - 2 = -1 \quad (20)$$

in three dimensions and

$$z = \frac{d}{3d-3} = \frac{1}{2} \quad (21)$$

also in three dimensions. The domain growth kinetics is then governed by the exponent  $n$  which is given by

$$n = \frac{z}{d} = \frac{1}{3d-3}. \quad (22)$$

Our observed value of  $n \approx 0.17$  agrees quite well with the theoretical prediction. In addition, we note that this same growth exponent has recently been observed in experiments on depletion driven colloids.<sup>15</sup>

For denser systems (such as those shown in Fig. 9 for  $f=0.01$  and  $f=0.02$ ), the morphology of domains is similar to the interconnected structure seen in a typical spinodal decomposition of a liquid–liquid mixture. The structure factor data for these volume fractions show interesting features. Fits to the data in Figs. 10(a) and 10(b) show that  $S(q)$  is consistent with Porod's law [ $S(q) \sim q^{-4}$ ] for large  $q$  values while for intermediate values of  $q$ ,  $S(q) \sim q^{-D_f}$  with  $D_f \approx 1.8$  consistent with the well-known DLCA value.<sup>28</sup> We see

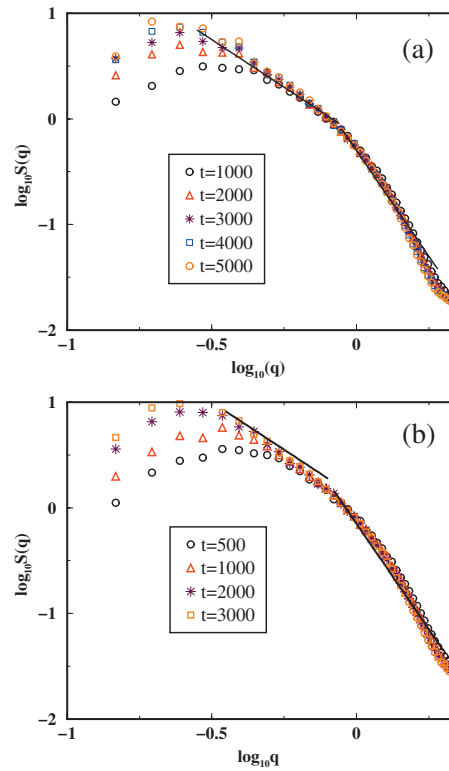


FIG. 10. (a) Log-log plot of the structure factor  $S(q,t)$  as a function of  $q$  at different times for  $U_m=4kT$ ,  $f=0.01$ , and  $\xi=0.1$ . Our results are consistent with Porod's law for large  $q$  values and for small  $q$  values; a slope of  $-1.8$  is consistent with the data. (b) Log-log plot of the structure factor  $S(q,t)$  as a function of  $q$  at different times for  $U_m=4kT$ ,  $f=0.02$ , and  $\xi=0.1$ . Our results are consistent with Porod's law for large  $q$  values and for small  $q$  values; a slope of  $-1.8$  is consistent with the data.

such hybrid morphology in Fig. 9 as well when we zoom in to the clusters: the growing clusters are compact at short length scales but are fractal-like at large length scales.<sup>29</sup>

Growth kinetics for these denser systems is still controlled by cluster-cluster interactions. As before, clusters do diffuse around until they meet each other. However, the clusters at these denser systems do not seem to coalesce into compact clusters when they meet but keep their ramified shape. Thus one would expect that the growth-law exponent would crossover to the irreversible limit, i.e., to the DLCA limit for dense systems.

In Figs. 11(a) and 11(b) we plot the number of clusters versus time in log-log plots for volume fractions  $f=0.01$  and  $f=0.02$ , respectively. For  $f=0.02$ ,  $N_c(t) \sim t^{-1}$  consistent with the DLCA value of  $z=1$  as discussed above. Note that if the clusters are compact and they would completely coalesce when they meet,  $z=1/2$  corresponding to the value of  $n=1/6$  seen before. It seems that for  $f=0.01$ , one gets an intermediate value of  $z \approx 0.75$ , in between the coalescence and the DLCA limit.

These conclusions are supported by the data for the radius of gyration as shown in Figs. 12(a) and 12(b). For  $f=0.02$ , one gets a clear-cut DLCA value for  $n=z/D_f=0.55$  with  $z=1$  and  $D_f=1.8$ , while for  $f=0.01$ , the growth exponent is yet to reach the DLCA limit and one finds an intermediate exponent of  $n \approx 0.4$ . This intermediate value of  $n \approx 0.4$ , however, is consistent with the intermediate value of  $z \approx 0.75$  seen before as  $n=z/D_f=0.75/1.8=0.42$ .

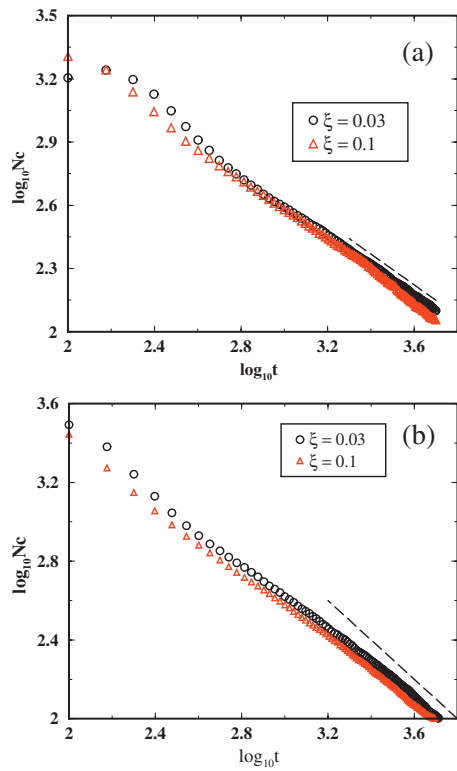


FIG. 11. (a) Log-log plot of the number of clusters  $N_c$  as a function of time for  $U_m=4kT$  and  $f=0.01$ . The dotted line with the slope of  $-0.75$  is a guide to the eyes. (b) Log-log plot of the number of clusters  $N_c$  as a function of time for a  $U_m=4kT$  and  $f=0.02$ . The dotted line with the slope of  $-1$  is a guide to the eyes.

We now provide estimation for the intermediate value of the growth exponent seen above. For this purpose we assume that the cluster growth kinetics is still controlled by a Binder–Stauffer mechanism but clusters do not coalesce completely when they meet each other. As a result clusters can be treated as fractals in the modified Binder–Stauffer scheme instead of treating them as compact objects. Equations (10) and (11) will still be valid but now  $R_g \sim N^{1/D_f}$  and hence

$$D_N \approx N^{2/D_f-2}. \quad (23)$$

The kernel  $K$  is then given by

$$K \sim D_N R_g \sim N^{(2/D_f)-2+(1/D_f)} \sim N^{3/D_f-2}, \quad (24)$$

yielding a homogeneity of  $\lambda = 3/D_f - 2$ , a kinetic exponent of

$$z = \frac{1}{1-\lambda} = \frac{D_f}{3D_f-3}, \quad (25)$$

and a growth exponent of

$$n = \frac{z}{D_f} = \frac{1}{3D_f-3}. \quad (26)$$

For  $D_f=1.8$ , one finds  $z=0.75$  and  $n=0.42$  in excellent agreement with our simulation results described above.

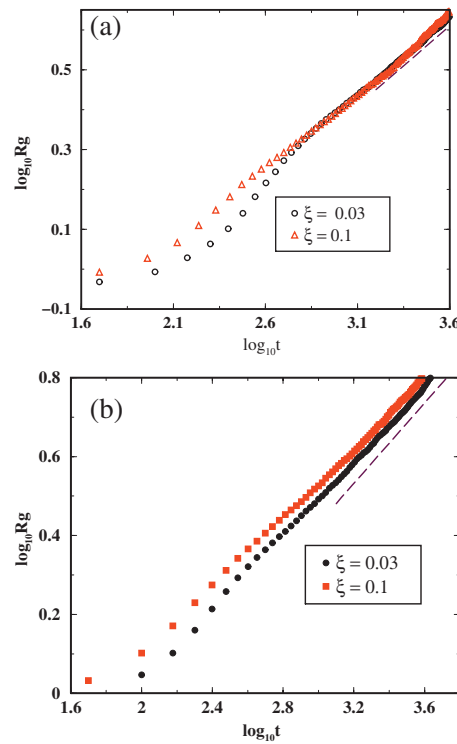


FIG. 12. (a) Log-log plot of radius of gyration  $R_g$  as a function of time for  $U_m=4kT$  and  $f=0.01$ . The dotted line with the slope of  $0.4$  is a guide to the eyes. (b) Log-log plot of radius of gyration  $R_g$  as a function of time for  $U_m=4kT$  and  $f=0.02$ . The dotted line with the slope of  $0.55$  is a guide to the eyes.

### C. Morphology and growth kinetics for deeper quenches

In this section we study morphology and growth kinetics of clusters for a deep quench characterized by  $U_m=10kT$  and  $\xi=0.1$ . Snapshots of the system for two different volume fractions  $f=0.002$  and  $f=0.02$  are shown in Fig. 13. As observed in Fig. 13(b), now the clusters have fractal morphology even at very low volume fractions. Also, noteworthy is the fact that the zoomed-in version of a typical cluster of the system [Fig. 13(d)] shows much weaker short-range crystall-

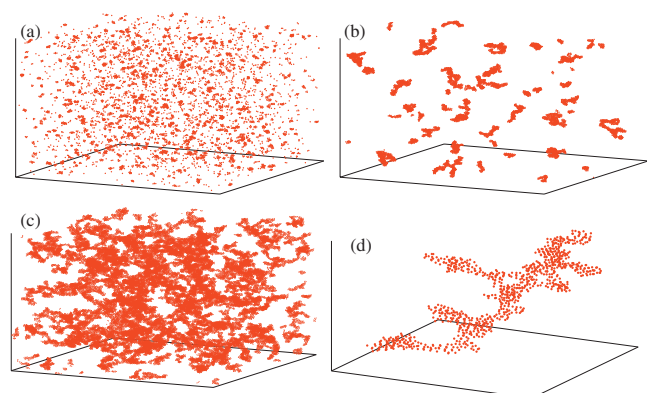


FIG. 13. Snapshots of deep quenched ( $U_m=10kT$ ) systems for two different volume fractions. (a) and (b) are for a volume fraction  $f=0.002$  at  $t=250$  and  $t=10000$ , respectively. (c) is for  $f=0.02$  at  $t=5000$  while (d) shows the zoomed-in version of a typical cluster of the system shown in (c). Short-range crystalline order in the zoomed-in cluster of (d) is much weaker than the ones seen, for example, in Figs. 9(b) and 9(d).

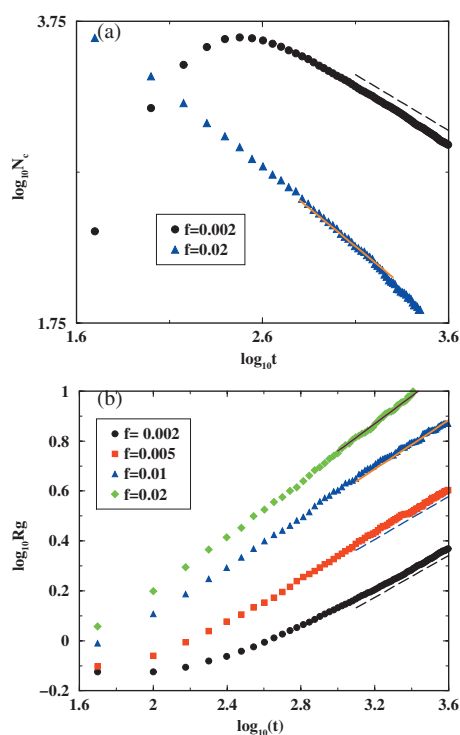


FIG. 14. (a) Log-log plot of the number of clusters  $N_c$  as a function of time for a deep quenched system of  $U_m=10kT$  at  $f=0.002$  and  $f=0.02$ , respectively. The kinetic exponents computed from the slopes of these graphs are  $z=0.75$  and  $z=1$ , respectively. (b) Log-log plot of radius of gyration  $R_g$  as a function of time for a  $10kT$  deep quenched system with  $\xi=0.1$  for four different values of the volume fraction  $f$ :  $0.002$ ,  $0.005$ ,  $0.01$ , and  $0.02$ . The growth exponents  $n$  for these volume fractions are given by  $n=0.4$ ,  $0.43$ ,  $0.5$ , and  $0.55$ . The growth exponent at low volume fractions is consistent with the intermediate regime scaling value of  $n\approx 0.42$  discussed in the text while for larger volume fractions one asymptotically obtains the pure DLCA value of  $n=0.55$ .

line order than seen in clusters for  $4kT$  quenches shown in Figs. 9(b) and 9(d), for example. This is expected as for deeper quenches, colloidal particles do not break as often from the parent cluster and thus get stuck in low coordination number sites.

Growth kinetics in this case crosses over to the DLCA limit as the volume fraction is increased. For a dilute system characterized by  $f=0.002$ , the kinetic exponent is given by  $z\approx 0.75$  consistent with our scaling analysis for the intermediate regimes [Fig. 14(a)]. It is interesting to note that for this deep quench, the intermediate regime result applies to much smaller volume fractions than for the  $4kT$  quench analyzed before. The kinetic exponent takes on a pure DLCA value of  $z=1$  for  $f=0.02$ .

The evolution of the growth exponent  $n$  with volume fractions is depicted in Fig. 14(b). For low volume fractions, we again obtain the intermediate value of the growth exponent given by  $n\approx 0.42$  while for larger volume fractions, the growth exponent is given by a pure DLCA value of  $n=0.55$ .

#### IV. SUMMARY AND CONCLUSIONS

In summary, we have carried out extensive BD simulations to study cluster morphology and growth kinetics in quenched short-range attractive colloidal systems. The model

potential we have studied here is given by the AOV depletion interaction. However, we expect that our results would apply for general short-range attractive potentials.

For very low volume fractions and shallow quench depths, we have studied the morphology of the growing crystals in terms of various bond orientational order parameters. The nucleating crystals are quite liquidlike at early times. At late times, the core of the crystal is characterized by a close-packed symmetry (mixture of fcc and hcp) while the surface of the crystal at late times is liquidlike. We have not seen any evidence of a bcc structure at early times or at the surface of the growing crystal.

As the volume fraction is increased for a shallow quench, cluster-cluster interactions control the growth kinetics. For low volume fractions, clusters seem to diffuse following a mechanism described by Binder and Stauffer many years ago. When two clusters meet each other, they coalesce and clusters remain compact. In this regime the growth-law exponent agrees well with Binder–Stauffer predictions and with recent experimental results.

When volume fractions are increased further, clusters do not have time to completely coalesce when they meet each other. Clusters show hybrid morphology now: ramified on large length scales but close-packed crystalline at short length scales. We have extended the Binder–Stauffer mechanism to explain the observed growth kinetics for this intermediate regime. Such an intermediate value of the growth exponent ( $n\approx 0.42$ ) has not been observed in experiments yet and our simulations would motivate further experimental studies.

For deeper quenches, clusters are fractals even at low volume fractions and the intermediate value of the kinetic exponent is observed even at very low volume fractions. When volume fractions are increased further, the growth kinetics asymptotically reaches the DLCA limit.

#### ACKNOWLEDGMENTS

This work was supported by NSF NIRT Grant No. CTS0609318. We thank Professor C. Aakeroy, Professor J. Gunton, Professor K. Klabunde, and Professor B. M. Law for many useful discussions.

<sup>1</sup> W. C. K. Poon and M. D. Haw, *Adv. Colloid Interface Sci.* **73**, 71 (1997); V. J. Anderson and H. N. W. Lekkerkerker, *Nature (London)* **416**, 811 (2002).

<sup>2</sup> O. C. Compton and F. E. Osterloh, *J. Am. Chem. Soc.* **129**, 7793 (2007); B. Abécassis, F. Testard, and O. Spalla, *Phys. Rev. Lett.* **100**, 115504 (2008); H. Yan, S. Cingarapu, K. J. Klabunde, A. Chakrabarti, and C. M. Sorensen, *ibid.* **102**, 095501 (2009).

<sup>3</sup> P. R. ten Wolde and D. Frenkel, *Science* **277**, 1975 (1997); A. Fortini, E. Sanz, and M. Dijkstra, *Phys. Rev. E* **78**, 041402 (2008).

<sup>4</sup> See, for example, P. Charbonneau and D. R. Reichman, *Phys. Rev. E* **75**, 011507 (2007).

<sup>5</sup> See, for example, J. D. Gunton, M. San Miguel, and P. S. Sahni, in *Phase Transitions and Critical Phenomena*, edited by C. Domb and J. L. Lebowitz (Academic, New York, 1983), Vol. 8.

<sup>6</sup> A. G. Walton, *The Formation and Properties of Precipitates* (Interscience, New York, 1967); A. E. Nielsen, *Kinetics of Precipitation* (Pergamon, Oxford, 1964).

<sup>7</sup> *Kinetics of Aggregation and Gelation*, edited by F. Family and D. Landau (North-Holland, Amsterdam, 1984).

<sup>8</sup> For a review, see E. Zaccarelli, *J. Phys.: Condens. Matter* **19**, 323101 (2007).

- <sup>9</sup>A. J. Liu and S. R. Nagel, *Nature (London)* **396**, 21 (1998).
- <sup>10</sup>V. Trappe, V. Prasad, L. Cipelletti, P. N. Segre, and D. A. Weitz, *Nature (London)* **411**, 772 (2001).
- <sup>11</sup>E. K. Hobbie, *Phys. Rev. Lett.* **81**, 3996 (1998).
- <sup>12</sup>C. M. Sorensen, H. X. Zhang, and T. W. Taylor, *Phys. Rev. Lett.* **59**, 363 (1987).
- <sup>13</sup>E. H. A. de Hoog, W. K. Kegel, A. van Blaaderen, and H. N. W. Lekkerkerker, *Phys. Rev. E* **64**, 021407 (2001).
- <sup>14</sup>J. R. Savage, D. W. Blair, A. J. Levine, R. A. Guyer, and D. A. Dinsmore, *Science* **314**, 795 (2006).
- <sup>15</sup>P. J. Lu, E. Zaccarelli, F. Ciulla, A. B. Schofield, F. Sciortino, and D. A. Weitz, *Nature (London)* **453**, 499 (2008).
- <sup>16</sup>F. Cardinaux, T. Gibaud, A. Stradner, and P. Schurtenberger, *Phys. Rev. Lett.* **99**, 118301 (2007); T. Gibaud and P. Schurtenberger, *J. Phys.: Condens. Matter* **21**, 322201 (2009).
- <sup>17</sup>K. Kroy, M. E. Cates, and W. C. K. Poon, *Phys. Rev. Lett.* **92**, 148302 (2004); J. Bergenholtz, W. C. K. Poon, and M. Fuchs, *Langmuir* **19**, 4493 (2003); A. M. Puertas, M. Fuchs, and M. E. Cates, *J. Phys.: Condens. Matter* **19**, 205140 (2007).
- <sup>18</sup>K. G. Soga, J. R. Melrose, and R. C. Ball, *J. Chem. Phys.* **108**, 6026 (1998); K. G. Soga, J. R. Melrose, and R. C. Ball, *ibid.* **110**, 2280 (1999).
- <sup>19</sup>R. J. M. d'Arjuzon, W. Frith, and J. R. Melrose, *Phys. Rev. E* **67**, 061404 (2003).
- <sup>20</sup>D. Costa, P. Ballone, and C. Caccamo, *J. Chem. Phys.* **116**, 3327 (2002).
- <sup>21</sup>J. J. Cerdá, T. Sintes, C. M. Sorensen, and A. Chakrabarti, *Phys. Rev. E* **70**, 011405 (2004); **70**, 051405 (2004).
- <sup>22</sup>G. Foffi, C. Michele, F. Sciortino, and P. Tartaglia, *Phys. Rev. Lett.* **94**, 078301 (2005).
- <sup>23</sup>M. G. Noro and D. Frenkel, *J. Chem. Phys.* **113**, 2941 (2000).
- <sup>24</sup>S. Asakura and F. Oosawa, *J. Chem. Phys.* **22**, 1255 (1954).
- <sup>25</sup>A. Vrij, *Pure Appl. Chem.* **48**, 471 (1976).
- <sup>26</sup>K. Binder and D. Stauffer, *Phys. Rev. Lett.* **33**, 1006 (1974).
- <sup>27</sup>K. Binder and M. H. Kalos, *J. Stat. Phys.* **22**, 363 (1980).
- <sup>28</sup>R. Jullien and R. Botet, *Aggregation and Fractal Aggregates* (World Scientific, Singapore, 1987).
- <sup>29</sup>A. T. Skjeltorp, *Phys. Rev. Lett.* **58**, 1444 (1987).
- <sup>30</sup>A. Chakrabarti, D. Fry, and C. M. Sorensen, *Phys. Rev. E* **69**, 031408 (2004).
- <sup>31</sup>W. F. Van Gunsteren and H. J. C. Berendsen, *Mol. Phys.* **45**, 637 (1982).
- <sup>32</sup>N. Q. Nguyen and A. J. C. Ladd, *Phys. Rev. E* **66**, 046708 (2002); J. F. Brady, *J. Chem. Phys.* **99**, 567 (1993); D. O. Riese, G. H. Wegdam, W. L. Vos, R. Sprik, D. Fenistein, J. H. H. Bongaerts, and G. Grüberl, *Phys. Rev. Lett.* **85**, 5460 (2000).
- <sup>33</sup>J. R. Melrose, *Europhys. Lett.* **19**, 51 (1992).
- <sup>34</sup>M. Dijkstra, J. M. Brader, and R. Evans, *J. Phys.: Condens. Matter* **11**, 10079 (1999).
- <sup>35</sup>H. N. W. Lekkerkerker, W. C. K. Poon, P. N. Pusey, A. Stroobants, and P. B. Warren, *Europhys. Lett.* **20**, 559 (1992).
- <sup>36</sup>J.-x. Yang, H. Gould, W. Klein, and R. D. Mountain, *J. Chem. Phys.* **93**, 711 (1990).
- <sup>37</sup>P. L. Steinhardt, D. R. Nelson, and M. Ronchetti, *Phys. Rev. B* **28**, 784 (1983).
- <sup>38</sup>S. Auer and D. Frenkel, *Adv. Polym. Sci.* **173**, 149 (2005) and references therein.
- <sup>39</sup>F. Sciortino, P. Tartaglia, and E. Zaccarelli, *J. Phys. Chem. B* **109**, 21942 (2005).
- <sup>40</sup>C. Patrick Royall, S. R. Williams, T. Ohtsuka, and H. Tankaka, *Nature Mater.* **7**, 556 (2008).
- <sup>41</sup>U. Gasser, E. R. Weeks, A. Schofield, P. N. Pusey, and D. A. Weitz, *Science* **292**, 258 (2001).
- <sup>42</sup>P. R. ten Wolde, M. J. Ruiz-Montero, and D. Frenkel, *Phys. Rev. Lett.* **75**, 2714 (1995).
- <sup>43</sup>S. Alexander and J. McTague, *Phys. Rev. Lett.* **41**, 702 (1978).
- <sup>44</sup>O. Glatter and O. Kratky, *Small-Angle X-ray Scattering* (Academic, London, 1982).
- <sup>45</sup>H. Furukawa, *Adv. Phys.* **34**, 703 (1985).
- <sup>46</sup>M. Smoluchowski, *Phys. Z.* **17**, 557 (1916).
- <sup>47</sup>S. K. Friedlander, *Smoke, Dust, and Haze: Fundamentals of Aerosol Behavior* (Wiley, New York, 1977).
- <sup>48</sup>D. Fry, T. Sintes, A. Chakrabarti, and C. M. Sorensen, *Phys. Rev. Lett.* **89**, 148301 (2002).
- <sup>49</sup>F. Pierce, C. M. Sorensen, and A. Chakrabarti, *Phys. Rev. E* **74**, 021411 (2006).